Strength and toughness trade-off optimization of nacre-like ceramic composites

Kaoutar Radi, David Jauffrès, Sylvain Deville, Christophe L. Martin

Strength and toughness trade-off optimization of nacre-like ceramic composites

Kaoutar Radi [a,*], David Jauffres [a], Sylvain Deville [b], Christophe L. Martin [a]

[a] Univ. Grenoble Alpes, CNRS, Grenoble INP, SIMaP, F-38000, Grenoble, France
[b] Laboratoire de Synthèse et Fonctionnalisation des Céramiques, UMR 3080, CNRS/Saint-Gobain CREE, Saint-Gobain Research Provence, Cavaillon, France

Bio-inspired by abalone nacre, all ceramic brick-and-mortar composites with impressive mechanical properties have been recently manufactured. Albeit comprising only brittle constituents, extrinsic reinforcement mecha-nisms impart to these nacre-like ceramics high toughness and non-catastrophic crack propagation properties. While several models have been developed to understand the mechanical properties of natural and synthetic brick-and-mortar materials, they have always considered a ductile interface and focused mostly on intrinsic toughening mechanisms. Modeling so far has not captured the extrinsic toughening mechanisms responsible for the properties of nacre-like ceramics. Here we show that the Discrete Element Method (DEM) can account for reinforcement mechanisms such as microcracking and crack deflection, and quantitatively assess strength, initiation toughness and crack growth toughness. Two approaches are studied to enhance strength and toughness of nacre-like ceramics, either by reinforcing the interface globally (an increase of the interface strength) or locally (addition of nano-bridges). We combine the results to provide design guidelines for synthetic brick-and- mortar composites comprising only brittle constituents.

1. Introduction

The nacreous part of many seashells species is a composite which toughness is several orders of magnitude larger than its components [1, 2]. Nacre has a brick-and-mortar (BM) architecture–aligned mineral tablets (bricks) linked together by a thin organic interface (mortar)–that provides cohesion and energy dissipation capacities to the material [3, 4]. Other structural features are found within the architecture of nacre, from the fibril network of the interface to the arrangement of mesolayers [5]. The high toughness of nacre can be attributed to different reinforcement mechanisms present at different length scales.

Reinforcement mechanisms can be classified as either intrinsic or extrinsic. Intrinsic mechanisms, acting ahead of the crack tip, result mainly from plasticity and are active independently of the crack size or geometry. They essentially affect crack initiation toughness [6]. In contrast to intrinsic toughening, extrinsic toughening includes microstructural mechanisms that act behind the crack tip to resist its further opening by lowering the stress and strain fields at the crack tip. These mechanisms can occur by fiber bridging, where the fibers hold the two fracture surfaces together after the crack has propagated, or by frictional sliding or interlocking between two rough fracture surfaces. It can also be a result of microcracking around the main crack to relieve the stress at the crack tip. Extrinsic mechanisms influence only the crack growth [7,8]. A clear manifestation of this dependence is the rising resistance curve (R-curve) where the force to sustain cracking increases with the crack extension [7,9].

Inspired by nature, many synthetic BM materials have been developed [10–15]. Because the mortar that provides the necessary plastic deformation in these composites is a metal or a polymer, the composites cannot withstand harsh environmental conditions (high temperatures, oxidation, etc …). In contrast, the nacre-like alumina processed by Bouville et al. [16], Le Ferrand et al. [17] or Pelissari et al. [18] are only composed of brittle inorganic constituents (e.g. 98.5 vol% of alumina tablets and nano-particles, 1.3 vol% of silica and 0.2 vol% of Calcia for the composite developed by Bouville et al.). These ceramic-ceramic composites can thus retain high strength and high toughness at high temperature (600 °C), which makes them very attractive materials for aeronautics, energy, or defense applications. Bouville et al. have reproduced some of the above reinforcement mechanisms (crack deflection, microcracking, tablet pull-out, etc …), and showed the essential role of alumina nano-particles at the interface that forms nano-bridges between the tablets, providing energy dissipation

* Corresponding author.
E-mail address: kaoutar8radi@gmail.com (K. Radi).

mechanisms during crack propagation. Modeling the various mechanisms that explain how a composite which comprises only brittle mineral constituents becomes damage-resistant should help to optimize the material. Indeed, nacre-like ceramics material may still be far from their optimum as only a few microstructural designs have been tested. Adequate modeling should guide microstructural design and help to further improve this material.

The effect of the microstructure on strength and toughness in BM materials with ductile mortar has been approached by several analytic shear-lag models that use a Representative Element Volume (RVE). Stiffness, strength and energy absorption were predicted as a function of microstructural parameters [19–23], and key parameters were introduced to optimize the material and achieve simultaneously high stiffness, strength and energy absorption [22]. Sophisticated shear-lag model can also account for crack bridging [24] but other extrinsic mechanisms such as microcracking or crack deflection were approached by numerical models. Early numerical efforts were based on Finite Element Modeling (FEM) [25,26] or discrete lattice [27,28]. More recently, a discrete element approach using rigid brick elements with cohesive zone interactions was developed [29,30]. The use of rigid elements is numerically very efficient but implicitly makes the assumption that bricks are unbreakable and that the two constituents have a very large stiffness contrast. Pro et al. have shown that the plastic zone developing ahead of the crack tip increases with interface ductility [29], and that consequently the modeling of typical natural or synthetic BM materials with ductile interface requires a very large volume. On the contrary, the process zone ahead of the crack tip should be limited to a smaller volume in the case of elastic-brittle interfaces [31]. The numerical efficiency of the rigid brick approach has allowed Abid et al. to investigate large volumes and assess the R-curve of BM materials with elastic-softening or elastic-plastic interfaces [31]. However, the results and conclusions provided by this type of model cannot be directly transposed to the case of nacre-like ceramic with brittle interfaces and a mild stiffness contrast between the two constituents.

Many authors have underlined the important role of nano-bridges between tablets in bio-inspired materials [15,32–35]. However, the inclusion of nano-bridges in BM analytical or numerical models is scarce [26,36].

Originally designed for granular materials [37–39], and extended more recently to continuous materials [40–43] the Discrete Element Method (DEM) based on spherical elements can naturally elucidate topological modifications (crack propagation, multiple cracking, crack branching, etc …), which makes it appropriate to model extrinsic reinforcement mechanisms. In contrary to cohesive zones modeling, the crack path location does not need to be predefined in DEM. This means that considering breakable tablets is not more expensive computationally. Also, after fracture, particles may resume contact and interact via frictional contacts. Several studies have proven that DEM is well suited to model the fracture behavior of elastic-brittle materials [42,44–46]. Recently, DEM simulations at the scale of one nacre-like ceramic RVE were successfully validated against existing analytical models in terms of elasticity and strength. The propagation of the crack within the RVE itself was modeled demonstrating the added value of DEM for this problem. Compared to the discrete approach with rigid bricks, the DEM model can capture friction and interlocking effects within an interface and the propagation of the crack to a brick. Fracture surfaces of nacre-like ceramics exhibit broken tablets [16], demonstrating that the eventuality of brick breakage should be accounted for.

In this work, we use DEM to reproduce extrinsic and intrinsic toughening mechanisms of all-ceramic composites at the scale of a hundred tablets and study the impact of interface reinforcement on strength and toughness. The article is organized as follows. First, the DEM framework is introduced briefly and the setup of the microstructure and the simulations are outlined. Special attention is given to explain the R-curve computation. Second, the influence of two strategies to reinforce the interface, namely the increase of nominal strength of the interface and the addition of nano-bridges is studied. The capacity of this modeling approach to capture damage and crack propagation is highlighted. The results are then gathered in property maps that provide design guidelines.

2. Discrete model for brick-and-mortar materials

2.1. DEM framework

To model the mechanical behavior of continuous media with DEM, we consider the material as a random packing of spherical particles bonded by cylindrical beams. The particles here have no physical meaning and should only be regarded as entities of discretization, similar to the mesh in FEM. The DEM formulation and the sample generation procedure are similar to our earlier study on a Representative Volume Element [47]. All DEM simulations are performed with our in-house code dp3D [48]. The bonding laws that connect the particles which model both the interface and the tablet are described in section S1 of the Supporting Information (SI). The strength of bonds is dictated by the Rankine criterion.

2.2. Generation of numerical microstructures and calibration

Fig. 1 shows a schematic of the typical BM microstructure used in this work. The generation procedure for BM microstructure has been described in earlier works [43,47] and is detailed in section S2 of the SI. A zoom-in (Fig. 1) shows the structural parameters of the RVE used. Tablets of length L and thickness t_t are connected horizontally and vertically by thin (red) interfaces with thickness t_i. The BM microstructure is defined by three non-dimensional parameters: the tablet's aspect ratio $\rho = \frac{L}{t_t}$, the overlap ratio $k = \frac{L_0}{L_t}$ and the tablet volume fraction $\varphi = \frac{t_t}{t_t+t_i}$. The microstructural parameters used in this study mimic the ceramic material described by Bouville et al. [16] with an aspect ratio $\rho = 14$ and a tablet's volume fraction $\phi = 0.876$. The tablet volume fraction was chosen to have at least three particles at the interface to ensure convergence [47]. Increasing the tablet volume fraction means increasing the overall number of particles, which leads to prohibitive CPU time. The overlap ratio $k = 0.25$ was chosen under the assumption that there is a uniform distribution over $0 < k < 0.5$.

Tablets and interfaces in the microstructure (Fig. 1) are represented by a given particle type assigned with microscopic parameters to model their respective mechanical behavior. The stiffness of bonds that connect interface and tablet particles are treated in series (see Eq. S(2) in section S2 of the SI) and their values are calibrated following the method described in Ref. [43]. As for fracture, the strength of bonds at the interface-tablet junction is dictated by the lowest strength (i.e. interface material strength). The microscopic interaction parameters (particle level) are calibrated to attain the macroscopic properties of the interface and of the tablet as detailed in Ref. [47]. Table 1 summarizes the input parameters used in this study. For the Young's moduli, typical value for alumina (tablets), and a lower bound value for an oxide glass (interface) are used. Concerning strength, the tablet's value is based on the study of Feilden et al. [49]. For the interface, a large interval of strength is used as there is no clear indication on the actual accessible values. The resulting mechanical macroscopic response of a nacre RVE is comparable.

In terms of elasticity and stress at crack initiation with existing analytical models, thus validating the DEM approach [47].

2.3. DEM simulations

Two types of numerical tests were performed: uniaxial tensile loading of unnotched samples, to study tensile strength and of notched samples (Fig. 1) to study toughness. The number of particles used to mesh the samples is 1 280 000. This value is based on the discretization

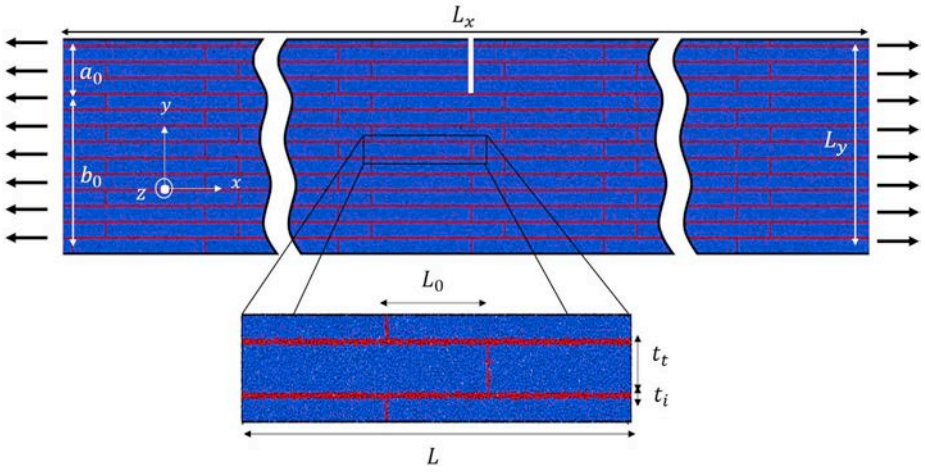

Fig. 1. Overview of a notched microstructure with staggered tablets (in blue) showing geometry, dimensions (L_x = 57 μm, L_y = 9 μm), and loading. Similar unnotched samples are used for strength determination. Only half of the volume, used in our Simulations, is represented here. A close-up view shows a representative volume element together with characteristic structural parameters. (For interpretation of the references to colour in this figure legend, the reader is referred to the Web version of this article).

Table 1
Macroscopic parameters (E Young modulus, ν Poisson ratio, Σ macroscopic strength) used in the simulations. Indicia i and t are used hereafter to refer to the parameters of the interface and tablet, respectively.

	E	ν	Σ
Interface	40 GPa	0.2	0.1 − 2 GPa
Tablet	400 GPa	0.2	4 GPa

convergence study carried out previously [47]. Note that although 2D in its main geometrical features, our model is 3D, with several spheres in the z direction. The size of the samples is 5633 R × 900 R × 6 R where R = 10 nm is the particle radius.

The thickness of a tablet is 500 nm, comparable to the real nacre-like alumina [16]. Periodic boundary conditions in x and z directions were used with strain-rate imposed in the x direction. Free surface conditions were used in the y direction. Periodic boundary conditions in z correspond to a 2D plane strain configuration and only a few particles in z are required. Due to the periodic conditions in the x direction, crack interaction may arise in case of large crack deviation. The sample was thus chosen long enough in this direction ($\frac{L_x}{L_y}$ = 6.4) to retard this artificial effect.

Only one simulation per condition (Σ_i value, Nb value, …) was conducted. However, we evaluated the reproducibility of the results by generating five different initial random packings for a given typical case and the resulting standard deviation was less than 15%.

2.4. R-curve computation

The determination of fracture toughness involves tensile testing along the x axis of the notched microstructure (Fig. 1). During simulations, the deformation $_x$ was progressively increased to propagate a mode I crack through the numerical sample. At every output step i, the number of broken bonds, the projected crack length a_i and the tensile stress are calculated. The procedure to compute a_i is detailed in section S3 of the SI.

To assess the reinforcement that occurs during stable crack propagation, the critical stress intensity factor K_{Ic} versus the projected crack length was calculated (R-curve). Due to the absence of plasticity in our model (allceramic composite), the Griffith equation is used [50]:

$$K_{Ic}(a_i) = f\left(\frac{a_i}{L_y}\right)\Sigma(i)\sqrt{L_y} \tag{1}$$

where Σ is the macroscopic stress and L_y the size of the sample in the y direction. The expression of the function $f\left(\frac{a_i}{L_y}\right)$ depends on the specimen's geometry and the applied loading [51]. In our case, the samples are Single Edge Notched Tension (SENT) and the function $f\left(\frac{a_i}{L_y}\right)$ writes [50]:

$$f\left(\frac{a_i}{L_y}\right) = \frac{\sqrt{2\tan\left(\frac{\pi a_i}{2L_y}\right)}}{\cos\left(\frac{\pi a_i}{2L_y}\right)}\left[0.752 + 2.02\left(\frac{a_i}{L_y}\right) + 0.37\left(1 - \sin\left(\frac{\pi a_i}{2L_y}\right)\right)^3\right]$$

Most models use either the maximum, the minimum, or the average of the values on the R-curve to define toughness [31,52–54]. In this study, we determine for each simulation both the crack initiation toughness $(K_{Ic})_{init}$ and the maximum toughness $(K_{Ic})_{max}$ over the crack resistance curve and calculate the difference ΔK_{Ic}. The maximum critical stress intensity factor $(K_{Ic})_{max}$ is computed within the limit of a chosen value of the projected crack length ($a_i \leq 5$ μm).

As the crack propagation distance is very small (a few micrometers versus a few hundreds of micrometers experimentally), $(K_{Ic})_{max}$ is not representative of a typical crack growth toughness. Indeed, crack growth toughness is potentially much larger after the propagation of the crack over several hundreds of micrometers. Here, ΔK_{Ic} is proportional to the initial slope of the R-curve (Fig. S3. d in the SI) and is thus a more representative measure of the crack growth toughness.

3. Effect of global interface reinforcement via nominal strength

3.1. Macroscopic strength

Several samples with different interface strength values Σ_i $\left(\frac{1}{40} \leq \frac{\Sigma_i}{\Sigma_t} \leq \frac{1}{5}\right)$, were used with a fixed tablet strength Σ_t. A typical stress-strain plot is shown in Fig. 2a for $\Sigma_i = \frac{\Sigma_t}{8}$ with the axial stress and the total number of broken bonds vs. axial strain. Up to a strain value of ≈ 0.013%, the sample exhibits a linear stress-strain behavior characteristic of the elastic behavior of the BM structure prior to any significant fracture event. Between 0.013% and 0.020% strain, the amount of fracture events increases causing the failure of all vertical interfaces. After 0.032% strain, the sample fails in a catastrophic manner. The macroscopic strength Σ is defined by the maximum value of this curve.

The stress-strain responses of all tested samples are shown in Fig. 2b. Regardless of the interface strength, the deflection corresponding to the failure of vertical interfaces can be observed on all curves. Both failure stress and strain increase and then reach an asymptotic value at large Σ_i.

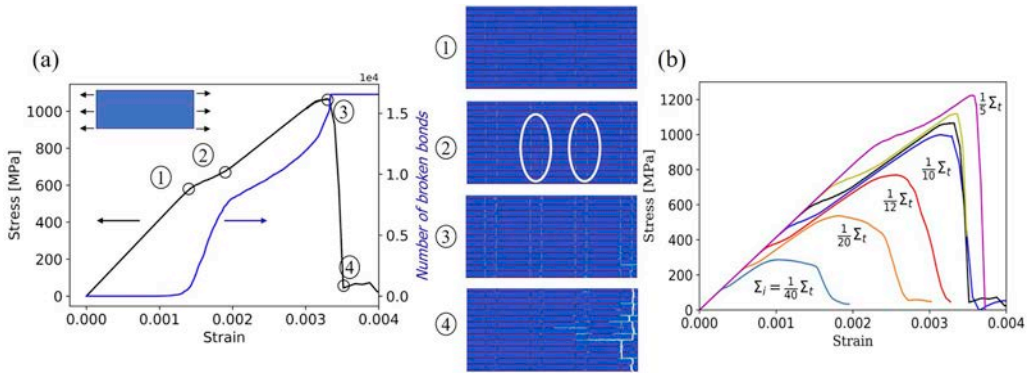

Fig. 2. a) A typical stress-strain curve along with the number of broken bonds and corresponding snapshots ($\sum_i = \frac{1}{8}\Sigma_t$ and ≈4400000 bonds) ① End of the elastic domain and failure initiation of vertical interfaces, ② failure of all vertical interfaces and initiation of crack growth in horizontal interfaces,③ stress maximum and ④ sample failure. The ellipsoids on the snapshots point to microcracking b) stress-strain evolution of unnotched samples with increasing interface strengths.

Albeit slightly lower, the asymptotic strength is comparable to the one predicted by a simple load transfer analysis ($\Sigma = \frac{\varphi\Sigma_t}{2} = 0.44\Sigma_t$) [22] and simulations at the scale of a RVE [47]. The maximum stress becomes more pronounced (more brittle behavior) as the interface strength approaches the tablet strength. We observed that the crack path goes from a stairway form at low interface strength to a straight one at high interface strength. In that case, we observe that some tablets are fracturing together with interfaces. The transition occurs around $\Sigma_i = \frac{1}{7}\Sigma_t$.

3.2. Toughness

Notched samples are used in this section to compute toughness (Fig. 1). Fig. 3 exemplifies the crack propagation by displaying the number of broken bonds for increasing strain and the corresponding stress-strain/broken bonds plots. The snapshots describe three characteristic steps in the simulation: ① damage initiation② maximum stress and ③ complete failure.

The examination of the failure patterns depicted in the snapshots of Fig. 3 helps understand the toughening mechanisms. For small interface strength, an overall non-catastrophic failure is observed (Fig. 3a). The vertical interfaces tend to fail early creating micro-cracking/multiple cracking [16,21]. This phenomenon occurs ahead of the crack tip and results in crack tip stress relaxation. Microcracking thus leads to an intrinsic reinforcement (as for plasticity in metals) and helps preserve a reasonable crack initiation toughness despite a very weak interface material. The main crack does not propagate through the material in a straight path. Instead, the crack propagates within the interface and is continually deflected when it encounters a tablet, resulting in a stairway pattern and crack bridging.

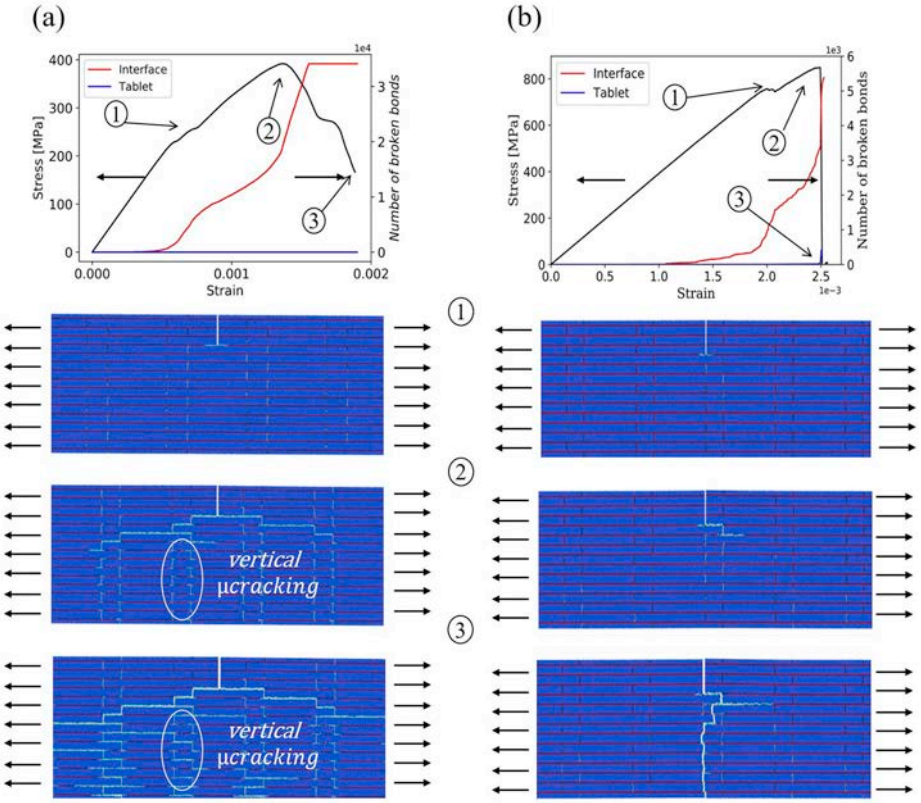

Fig. 3. Example of a notched sample under uniaxial loading for two different values of interface strength a)$\Sigma_i = \frac{1}{20}\Sigma_t$ and b) $\Sigma_i = \frac{1}{5}\Sigma_t$ with tensile stress-strain curves and broken bonds in both interface and tablets. Corresponding sequences of deformation show ① damage initiation, ② maximum stress and ③ material failure.

For high interface strength (Fig. 3b), a higher stress is needed to initiate interface failure, which leads to crack propagation in a straight manner into the material, as it becomes easier to break a tablet than to bypass it. In addition, very little micro-cracking is observed. The resulting crack initiation toughness is large but comes with an unstable crack propagation (Fig. 4). Note that in the extreme case of $\Sigma_i = \frac{1}{5}\Sigma_t$, no vertical interface breakage is noticed. In that case, the stress maximum follows damage initiation very closely.

Fig. 4 shows the resulting R-curve for three typical cases: low, intermediate, and high interface strength. The crack initiation toughness increases with interface strength. The first two cases are characterized by a rising R-curve in the form of a stairway and a relatively low crack initiation toughness. The third case exhibits a flat R-curve and a higher crack initiation toughness. The stairway pattern reveals the propagation of the crack in the interface by finite jumps: horizontal sections of the R-curve correspond to crack propagation in vertical interfaces occurring without any increase in stress (vertical interfaces are already broken) and vertical sections correspond to crack propagation in horizontal interfaces (stress increases but with a constant projected crack length). The length of the steps actually corresponds to a multiple of the platelet thickness. Abid et al. discrete brick model gives rise to very similar stairway R-curves [31].

Fig. 5 summarizes the preceding results by plotting strength, crack initiation toughness, and crack growth toughness (ΔK_{Ic}) as a function of interface strength. While crack initiation toughness and strength increase in a monotonic manner until they reach an asymptotic value, crack growth toughness reaches a maximum for $\Sigma_i = \frac{1}{10}\Sigma_t$, before decreasing.

Significant amount of microcracking and crack deflection can be noticed in the first two snapshots of Fig. 5, which occurs when it is more advantageous for the crack to deviate to reach weaker regions. On the other hand, the last two snapshots of Fig. 5 show a brittle behavior with little or no microcracking and limited crack deflection. This could be explained by the high shear strength of the interface that prevents interface damage, and subsequent sliding and friction prior to failure. An interesting configuration is achieved for $\Sigma_i = \frac{1}{10}\Sigma_t$, when the interface strength is high enough to ensure an optimal crack growth toughness combined with a relatively high strength and crack initiation toughness. Further increase of interface strength leads to higher strength but also to brittleness (significant drop of the crack growth toughness).

4. Effect of local interface reinforcement by nano-bridges

As demonstrated by evolution in mollusk nacre, nano-bridges represent a simple and potentially efficient route to reinforce locally the interface in a BM structure [55]. To test numerically the effect of nano-bridges on our samples, square bridges that span the whole depth of the sample in the z direction were installed in between two adjacent tablets. Nano-bridges have the same mechanical properties as the tablets. Although their geometry is simplistic ($h = d = t_i$, see Fig. S4 of the SI), it gives information on the efficiency of local reinforcement. The average number of nano-bridges per tablet (Nb) in the natural nacre is approximately 40 [56,57]. However, the density of nano-bridges in nacre-like alumina [16] is difficult to assess and not well controlled. In addition, the 2D nature of our model does not allow for a straightforward link between the number of nano-bridges per tablet in experimental conditions (3D) and the number of nano-bridges per tablet length in our simulation. Gu et al. [35] have shown that $Nb \approx 9$ is an optimal value for polymer-based 2D BM composites. Here, we choose to vary the number of bridges between $Nb = 3$ and $Nb = 18$ per tablet length.

The addition of bridges results in a slightly stiffer composite (2.4% increase for $Nb = 18$), because of the small increase in stiff material volume fraction.

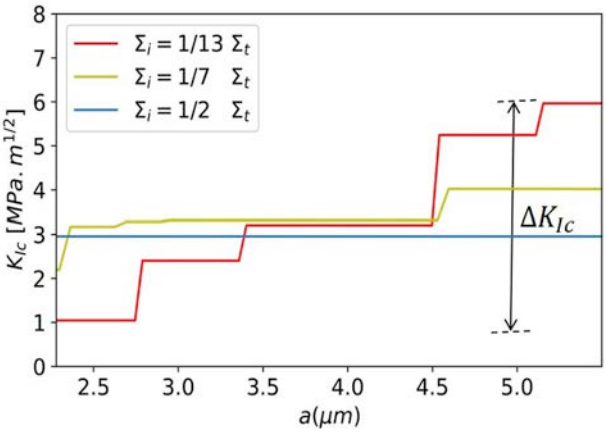

Fig. 4. Typical crack resistance curves for three interface values representing different behaviors: a rising curve with a staircase pattern for low interface strength, a constant K_{Ic} value for high interface strength and an intermediate case with moderate increase of.K_{Ic}.

4.1. Macroscopic strength

Using samples depicted in Fig. S4 of the SI with no initial notch, tensile tests were performed on nano-bridge reinforced microstructures. Fig. 6a and b show the strain-stress plots of samples for two different interface strengths. Fig. 6 a indicates that the number of bridges has a noticeable effect on the curve shape and maximum stress when starting from a low interface strength.

$\left(\Sigma_i = \frac{1}{20}\Sigma_t\right)$. The stress deflection that was characteristic of vertical interface failure in the specimen without nano-bridges is much less pronounced when bridges are introduced. More importantly, the maximum stress increases with the number of bridges. For a higher interface strength value (Fig. 6. b$\Sigma_i = \frac{1}{5}\Sigma_t$), the introduction of bridges still has a noticeable influence on strength but its effect is much less pronounced.

Fig. 6c aggregates the maximum stress values obtained with increasing Σ_i and increasing Nb. As already noticed for interface reinforcement by nominal strength, all curves converge towards a maximum strength of approximately 0.38 Σ_t, comparable but slightly lower than the load transfer analysis value $\left(\Sigma = \varphi\frac{\Sigma_t}{2} = 0.44\ \Sigma_t\right)$ [22]. Fig. 6c shows that, increasing the number of bridges is equivalent to an increase in interface strength when considering the macroscopic strength.

4.2. Toughness

The stress-strain responses of notched samples are presented for two different Nb's in Fig. 7. The $Nb = 6$ case shows the failure of vertical interfaces (vertical microcracking) that immediately transfers damage to the next horizontal interfaces and thus causes horizontal microcracking. The crack path is sinuous and characterized by an irregular surface compared to the 18-bridges sample. The presence of bridges (stiff material, high strength) interrupts the continuity of the interface (soft material, low strength) which allows for a more homogeneous stress distribution that leads to a more progressive failure.

Fig. 8. a summarizes the evolution of the crack initiation toughness with the number of bridges. $(K_{Ic})_{init}$ increases with the interface strength and the number of bridges up to $Nb = 18$. Fig. 8. a also shows that by reinforcing the interface homogeneously (0 Nb), the maximum value of $(K_{Ic})_{init}$ is close to tablet's toughness (see section S2 of the SI). However, this value is out-passed.

When adding bridges. In contrast with reinforcement via interface nominal strength where an asymptotic value is reached, the addition of bridges leads to a peak for $(K_{Ic})_{init}$ at $Nb = 18$. For larger Nb, $(K_{Ic})_{init}$ decreases back to the tablet's value.

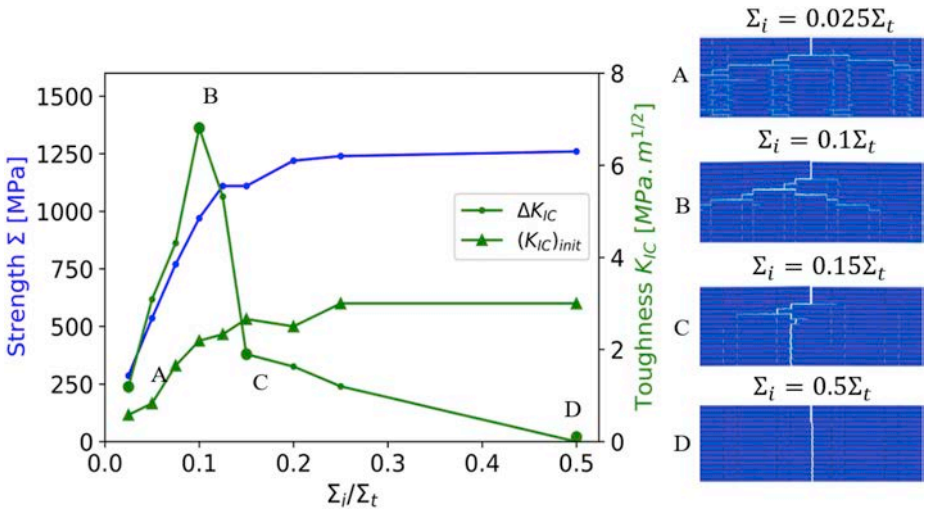

Fig. 5. Strength, crack initiation toughness, and crack growth toughness for different interface strengths with the crack propagation snapshots. $\Sigma_i = \frac{1}{10}\Sigma_t$ sample exhibits the largest improvement in both strength and toughness.

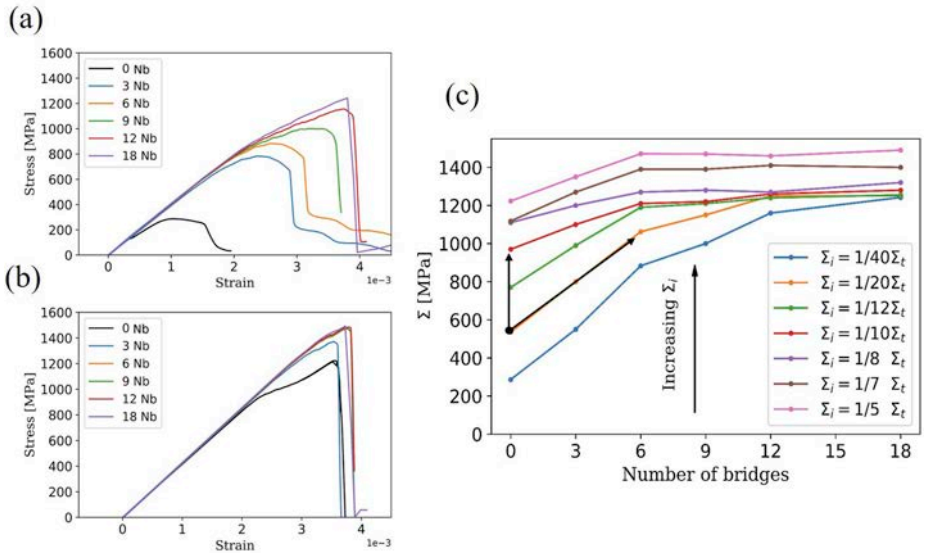

Fig. 6. Stress-strain response of unnotched samples with various number of bridges per tablet (Nb), for two different interface strengths, a) $\Sigma_i = \frac{1}{20}\Sigma_t$ and b) $\Sigma_i = \frac{1}{5}\Sigma_t$. c) Strength as a function of Nb for increasing interface strengths. The black arrows point to two different paths to obtain the same macroscopic strength either by an increase in Σ_i or the introduction of nano-bridges.

Fig. 8b shows the crack growth toughness as a function of the number of bridges for increasing interface strengths. For low interface strength, adding bridges increases crack growth toughness up to a maximum value before decreasing. The maximum value corresponds to a critical number of 6 bridges. For high Σ_i, the addition of bridges decreases the crack growth toughness. For example, adding bridges to the sample with an optimum crack growth toughness (i.e 0 Nb and $\Sigma_i = \frac{1}{10}\Sigma_t$) will only decrease the crack growth toughness value, however it is beneficial for crack initiation toughness (bold red curves on Fig. 8). The addition of bridges promotes microcracking and in turns an increase of crack growth toughness for low interface strength. However, adding bridges to an already strong interface is not beneficial for crack growth toughness as the interface becomes too strong to deflect efficiently the crack that runs through the tablets. By adding 18 bridges per tablet the amount of stiff material increases, which means that vertical interfaces failure controls the composite strength and the tablets fail immediately upon vertical interface rupture. For that extreme case, the high strength region is associated with a brittle composite response.

5. Discussion

The increase of the interface strength and the addition of bridges have a similar effect on strength (Fig. 6). In contrast, the interplay of interface strength and additional bridges is quite different on crack initiation toughness and crack growth toughness. The gain in crack initiation toughness by an increase in Σ_i is larger when starting from a microstructure with bridges than without bridges (Fig. 8). Microcraking events, which relax stress at the crack tip, disappear when increasing Σ_i for a sample without bridges. In contrast, we observed that samples with a large number of bridges still exhibit microcracking prior to crack propagation (Fig. 7b). More generally, the interface material is damaged but the nano-bridges remain intact while damage diffuses. This is because the stiffness ratio ($0\frac{E_i}{E_t} = 0.1$) is lower than the strength ratio ($\frac{\Sigma_i}{\Sigma_t}$) except for $\Sigma_i = \frac{1}{5}\Sigma_t$, where no microcracking is observed. The snapshots in Fig. 7b exemplify this phenomenon. The crack propagates first at the tip of the notch into a horizontal interface and encounters a bridge with a high stiffness and large strength, which will cause the crack to deviate

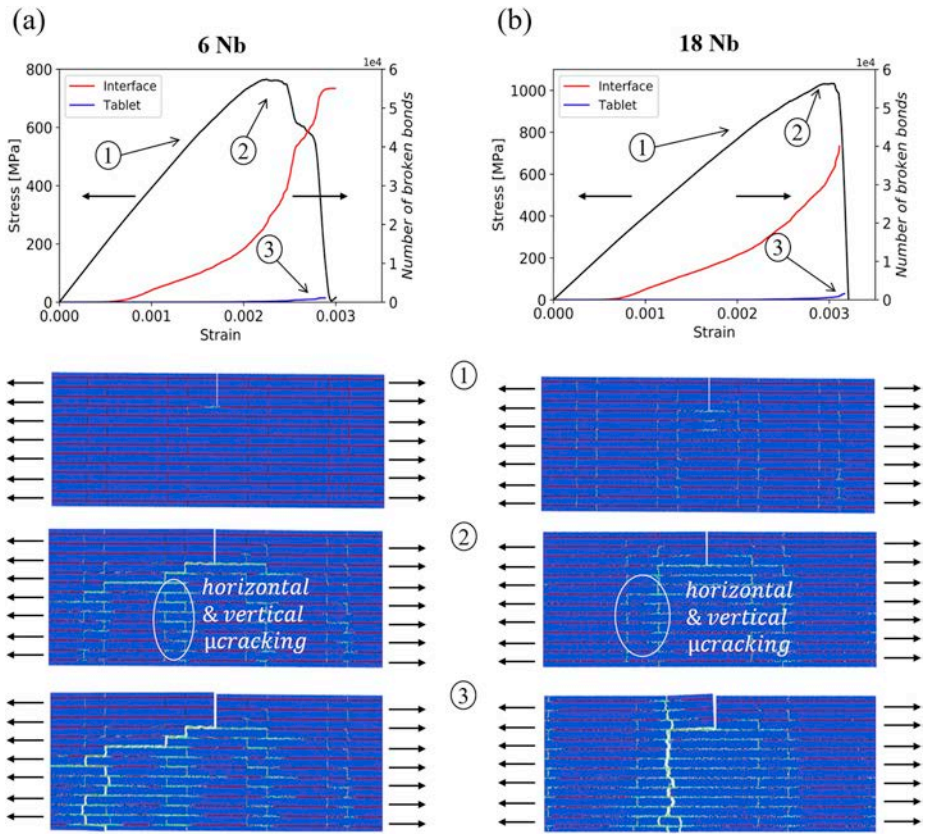

Fig. 7. An example of a notched sample under uniaxial loading for two different number of bridges per tablet a) 6 Nb and b) 18 Nb with a fixed interface strength $\Sigma_i = \frac{1}{20}\Sigma_t$.Tensile stress-strain plots and the corresponding sequences of deformation for both simulations with ① damage initiation, ② stress maximum, and ③ material failure.

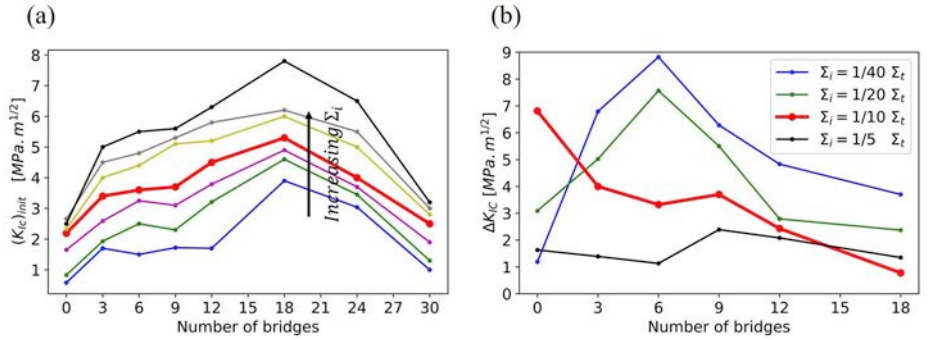

Fig. 8. Toughness of samples with different Nb compared to without bridges microstructures. a) crack initiation toughness and b) crack growth toughness as a function of *Nb* for an increasing interface strength. Red bold curves correspond to the optimal (for crack growth toughness) interface strength without bridges. (For interpretation of the references to colour in this figure legend, the reader is referred to the Web version of this article).

and propagate vertically into either the interface or the tablet. As for the crack growth toughness, although global or local reinforcement of the interface both leads to a maximum value before a decrease, the value reached via the addition of the optimal number of bridges (6) is slightly higher (9 MPa m$^{1/2}$ versus 7 MPa m$^{1/2}$). While large values of $(K_{Ic})_{init}$ are mainly related to the strength of the interface and micro-cracking development prior to crack propagation, large values of ΔK_{Ic} are also associated to crack deflection by the tablets that is less marked with nano-bridges (Fig. 7). The reason that localized reinforcement (addition of bridges) results into better properties than homogeneous reinforcement (increase of interface strength), could thus be explained by the additional horizontal microcracking that was not found in homogeneously reinforced samples, which leads to additional delocalization of stress. The microcracking that occurs before crack propagation contributes to the high value of crack initiation toughness, while microcracking after crack propagation contribute to high crack growth toughness.

From a practical point of view, starting with a low interface strength, composite strength Σ, initiation toughness $(K_{Ic})_{init}$ and crack growth toughness ΔK_{Ic} of nacre-like alumina can be increased either by an increase of the interface strength or the addition of alumina nano-bridges. For example, starting with $\Sigma_i = \frac{1}{20}\Sigma_t$ and no bridges, the material can be reinforced either by an increase of the interface strength to $\Sigma_i = \frac{1}{10}\Sigma_t$ or by the addition of 6 bridges to reach the same macroscopic strength $\Sigma_i = \frac{1}{4}\Sigma_t$ (see black arrows on Fig. 6). These two approaches (increase of Σ_i

from $\frac{1}{20}\Sigma_t$ to $\Sigma_i = \frac{1}{10}\Sigma_t$ or addition of 6 bridges) result in fine approximately in the same.

ΔK_{Ic} value (7–7.5 MPa $m^{1/2}$) and $(K_{Ic})_{init}$ value (2–2.5 MPa $m^{1/2}$) (Fig. 8). Reaching an optimum crack growth toughness by an homogeneous reinforcement of the interface only, would require a good control over the interface strength, which might seem difficult since the optimum interface strength range is quite narrow (Fig. 5). The control of bridges density seems more feasible experimentally. Combining interface strength $\Sigma_i = \frac{1}{40}\Sigma_t$ with 6 Nb, shows an interesting compromise between high strength and crack growth toughness (but with a modest $(K_{Ic})_{init}$ value).

The results presented above are gathered in two property maps to help optimize the design of BM materials made of brittle constituents. The first map shows strength versus crack initiation toughness (Fig. 9a), where it is evidenced that both high strength and high crack initiation toughness can be reached by an increase of interface strength and the addition of bridges (upper right region of the map). The second map shows strength versus crack growth toughness (Fig. 9b). The combination of both high strength and crack growth toughness can be obtained by reaching configurations on the right corner of the map. On the third map ΔK_{Ic} is plotted versus $(K_{Ic})_{init}$ in order to show the difficulty to combine high values for these two properties. By using these property maps, it is relatively clear how to combine either strength and crack initiation toughness or strength and crack growth toughness, depending on the desired application. When one looks for a combination of high strength and high crack initiation toughness, it is necessary to favor a microstructure with a large number of bridges and high interface strength. Conversely, a microstructure that combines a moderate number of bridges and a moderate interface strength leads to an optimum crack growth resistance. It is worth noting that the largest crack growth toughness value (9 MPa $m^{1/2}$) is obtained with the addition of bridges and cannot be reached with an increase of the nominal interface strength alone. The more complex case would be to combine high values for all three properties. In that case, a compromise must be found. For example, a microstructure with Nb = 9 and $\Sigma_i \approx 400$ MPa leads to reasonable values for strength, crack initiation toughness and crack growth toughness (Fig. 9c). The few experimental works available in the literature are qualitatively consistent with the presented property maps. For example, Bouville et al. [16] nacre-like alumina without nanobridges exhibits a strength comparable to alumina but a very.

Low toughness. In accordance with the property maps, Bouville et al. have shown that the bridges at the interface are essential to reach a high toughness with a low interface strength and Pelissari et al. have shown that the material could be further improved by using a stronger interface [18].

6. Conclusions

The interface that connects tablets plays an essential role in enhancing the mechanical performance of BM materials made of brittle constituents. In this study, we examined the effect of interface reinforcement on both strength and toughness using DEM simulations, we also proved the efficiency of DEM to reproduce important reinforcement mechanisms (microcracking and crack deflection).

The interface was reinforced using two different methods: either in a homogeneous manner, by an increase of its nominal strength, or by the addition of nano-bridges to the interface. At low interface strength, the un-notched samples were broken by tablets pull-out, whereas for high interface strength, samples were broken following a straight crack. Both reinforcements– increase of interface strength or addition of bridges–resulted in an increase of the overall strength until it reaches an asymptotic value which is in good accordance with analytic or numeric results at the scale of a single RVE [22,47].

We distinguished two toughness parameters: crack initiation toughness and crack growth toughness. We showed that the increase of interface strength increases crack initiation toughness until reaching a

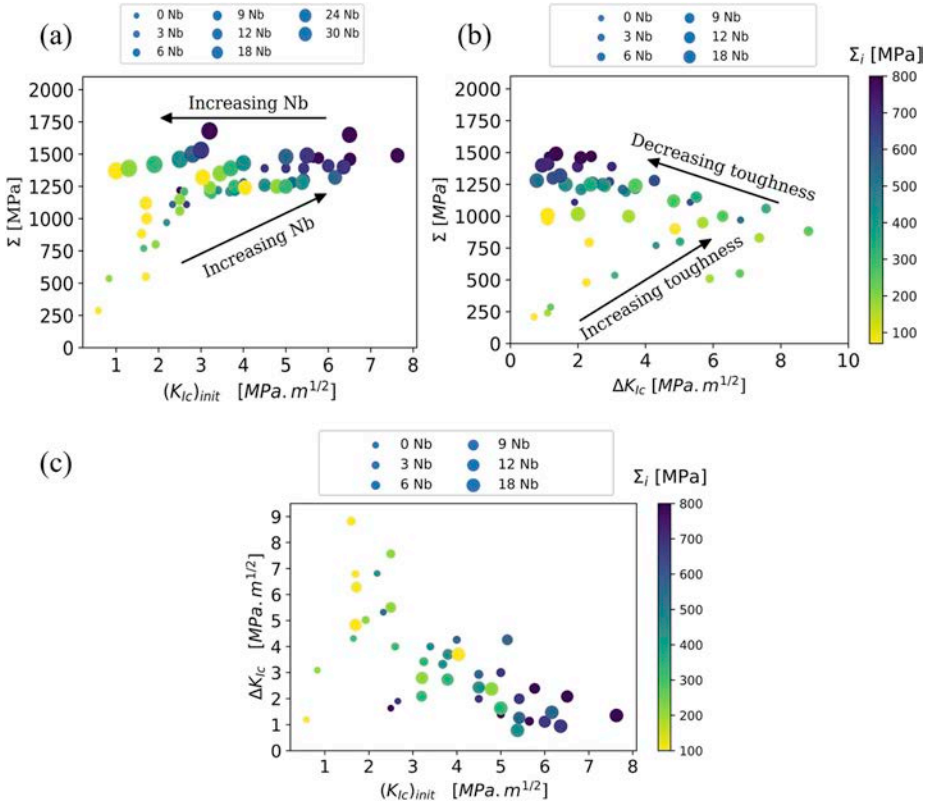

Fig. 9. Property maps showing the different possible combinations of strength and toughness by variation of either the interface strength or the addition of nano-bridges at the interface. a) crack initiation toughness, b) Crack growth toughness. c) Crack growth toughness versus crack initiation toughness.

maximum value. On the other hand, the increase of the density of alumina nano-bridges improves the crack initiation toughness value [15, 16] but only to decay after an optimum number of bridges. This result is consistent with the literature [33].

By studying the crack growth toughness, we demonstrate the important role of microcracking and crack deviation in increasing the crack growth toughness. An optimum value of crack growth toughness can be reached by adjusting the interface strength to $\Sigma_i = 0.1\Sigma_t$. This strength ratio is higher than the one used in experimental work [16,18], which would indicate that there is room for improvement in the design of BM materials made of brittle constituents.

On a more practical level, increasing the interface strength can be managed by changing the composition of the interface material during processing. A bi-layer system consisting of two sapphire substrates separated by an interface can be considered as a good candidate to tune and determine the interface properties experimentally. However, due to the narrow range of the optimum interface strength, the control seems complicated in practice. Controlling the density of alumina nano-bridges at the interface appears to be more feasible.

The model could be enriched to account for residual stresses within the interface, which are suspected to play an important role in the enhancement of mechanical properties of nacre-like ceramics developed by Pelissari et al. [18]. Besides, an extension to BM microstructures with ductile interfaces (metal or polymer) is possible by considering plastic interactions at the interface, knowing that DEM is also well-suited for tackling plastic deformations [48,58].

Our model has demonstrated its ability to capture complex damage and crack propagation within nacre-like ceramics. The use of this approach to model Ceramic Matrix Composites (CMCs), a class of material with only brittle constituents and similar damage and fracture behavior, could be of high interest.

Given the critical role of design for these materials, a question must be answered: do conclusions based on simulations of ideal microstructures apply to real materials? To answer this question, our next work will consist of making our model more realistic by taking into account randomness and initial defects of the material. This can be achieved by coupling EBSD micrographs of nacre-like alumina with DEM.

Acknowledgements

The Agence Nationale pour la Recherche (ANR -16- CE08-0006 BICUIT, program DS0303-2016) and the AGIR-POLE-PEM 2016 project (OMicroN) are greatly acknowledged for their financial support.

Appendix A. Supplementary data

Supplementary data to this article can be found online at https://doi.org/10.1016/j.compositesb.2019.107699.

References

[1] Chen P-Y, Lin a YM, Lin Y-S, Seki Y, Stokes a G, Peyras J, Olevsky E a, Meyers Marc André, Joanna McKittrick. Structure and mechanical properties of selected biological materials. J Mech Behav Biomed Mater jul 2008;1(3):208–26.
[2] Barthelat F, Espinosa HD. An experimental investigation of deformation and fracture of nacre-mother of pearl. Exp Mech 2007;47(3):311–24.
[3] Jackson AP, Vincent JFV, Turner RM. The mechanical design of nacre. Proc R Soc B Biol Sci 1988;234(1277):415–40.
[4] Espinosa Horacio D, Rim Jee E, Barthelat Francois, Buehler Markus J. Merger of structure and material in nacre and bone - perspectives on de novo biomimetic materials. Prog Mater Sci 2009;54(8):1059–100.
[5] Barthelat François, Yin Zhen, Buehler Markus J. Structure and mechanics of interfaces in biological materials. Nat. Rev. Mater. mar 2016;1(4):16007.
[6] Ritchie Robert O, Buehler Markus J, Paul Hansma. Plasticity and toughness in bone. American Institute of Physics; 2009.
[7] Ritchie Robert O. The conflicts between strength and toughness. Nat Mater 2011;10(11):817–22.
[8] Feng QL, Cui FZ, Pu G, Wang RZ, Li HD. Crystal orientation, toughening mechanisms and a mimic of nacre. Mater Sci Eng C 2000;11:19–25.
[9] Launey Maximilien E, Ritchie Robert O. On the fracture toughness of advanced materials. Adv Mater 2009;21(20):2103–10.
[10] Munch E, Launey ME, Alsem DH, Saiz E, Tomsia AP, Ritchie RO. Tough, bio-inspired hybrid materials. Science 2008;322(5907):1516–20.
[11] Oner Ekiz O, Dericioglu Arcan F, Kakisawa Hideki. An efficient hybrid conventional method to fabricate nacre-like bulk nano-laminar composites. Mater Sci Eng C 2009;29(6):2050–4.
[12] Zhao Hewei, Guo Lin. Nacre-inspired structural composites: performance-enhancement strategy and perspective. Adv Mater dec 2017;29(45):1702903.
[13] Yadav Ramdayal, Naebe Minoo, Wang Xungai, Kandasubramanian Balasubramanian. Review on 3D prototyping of damage tolerant interdigitating brick arrays of nacre. Ind Eng Chem Res 2017;56(38):10516–25.
[14] Tobias P. Niebel, florian Bouville, dimitri kokkinis, and andr?? R. Studart. Role of the polymer phase in the mechanics of nacre-like composites. J Mech Phys Solids 2016;96.
[15] Naglieri V, Gludovatz B, Tomsia AP, Ritchie RO. Developing strength and toughness in bio-inspired silicon carbide hybrid materials containing a compliant phase. Acta Mater 2015;(98):141–51.
[16] Bouville Florian, Maire Eric, Meille Sylvain, Van De Moortèle Bertrand, Stevenson Adam J, Deville Sylvain. Strong, tough and stiff bioinspired ceramics from brittle constituents. Nat Mater 2014;13(5):508–14.
[17] Le Ferrand Hortense, Bouville Florian, Niebel Tobias P, Studart André R. Magnetically assisted slip casting of bioinspired heterogeneous composites. Nat Mater sep 2015;14(September):1–17.
[18] Pedro IBGB, Pelissari Florian Bouville, Pandolfelli Victor C, Carnelli Davide, Finn Giuliani, Luz Ana P, Saiz Eduardo, Studart André R. Nacre-like ceramic refractories for high temperature applications. J Eur Ceram Soc 2017;38(4):2186–93.
[19] Kotha SP, Li Y, Guzelsu N. Micromechanical model of nacre tested in tension. J Mater Sci 2001;36(8):2001–7.
[20] Jäger Ingomar, Fratzl Peter. Mineralized collagen fibrils: a mechanical model with a staggered arrangement of mineral particles. Biophys J 2000;79(4):1737–46.
[21] Matthew R Begley, Philips Noah R, Compton Brett G, Wilbrink David V, Ritchie Robert O, Utz Marcel. Micromechanical models to guide the development of synthetic 'brick and mortar' composites. J Mech Phys Solids 2012;60(8):1545–60.
[22] Barthelat Francois. Designing nacre-like materials for simultaneous stiffness, strength and toughness: optimum materials, composition, microstructure and size. J Mech Phys Solids 2014.
[23] Ni Yong, Song Zhaoqiang, Jiang Hongyuan, Shu Hong Yu, He Linghui. Optimization design of strong and tough nacreous nanocomposites through tuning characteristic lengths. J Mech Phys Solids 2015;81:41–57.
[24] Yue Shao, Zhao Hong Ping, Feng Xi Qiao, Gao Huajian. Discontinuous crack-bridging model for fracture toughness analysis of nacre. J Mech Phys Solids 2012;60(8):1400–19.
[25] Katti Kalpana S, Katti Dinesh R, Pradhan Shashindra M, Bhosle Arundhati. Platelet interlocks are the key to toughness and strength in nacre. J Mater Res 2005;20:1097–100. 05.
[26] Katti Dinesh R, Pradhan Shashindra Man, S Katti Kalpana. Modeling the organic-inorganic interfacial NANOASPERITIES IN a model BIO-nanocomposite. NACRE 2004;6:162–8.
[27] Nukala Phani Kumar VV, Zapperi Stefano, Åimunović Sran. Statistical properties of fracture in a random spring model. Phys Rev E - Stat Nonlinear Soft Matter Phys 2005;71(6):1–11.
[28] Dimas Leon S, Buehler Markus J. Tough and stiff composites with simple building blocks. J Mater Res 2013;28(10):1295–303.
[29] William Pro J, Lim Rone Kwei, Petzold Linda R, Utz Marcel, Begley Matthew R. GPU-based simulations of fracture in idealized brick and mortar composites. J Mech Phys Solids 2015;(80):68–85.
[30] Abid Najmul, Mirkhalaf Mohammad, Barthelat Francois. Discreteelement modeling of nacre-like materials: effects of random microstructures on strain localization and mechanical performance. J Mech Phys Solids 2017;112:385–402.
[31] Abid Najmul, Pro J William, Barthelat Francois. Fracture mechanics of nacre-like materials using discrete-element models: effects of microstructure, interfaces and randomness. J Mech Phys Solids 2018;124:350–65.
[32] Gu Grace X, Leon Dimas, Zhao Qin, Buehler Markus J. Optimization of composite fracture properties: method, validation, and applications. J Appl Mech 2016;83(7):071006.
[33] Grossman Madeleine, Bouville Florian, Masania Kunal, Studart André R. Quantifying the role of mineral bridges on the fracture resistance of nacre-like composites. Proc Natl Acad Sci 2018:24–8. June.
[34] Grossman Madeleine, Bouville Florian, Erni Florian, Masania Kunal, Libanori Rafael, André R. Studart. Mineral nano-interconnectivity stiffens and toughens nacre-like composite materials. Adv Mater 2017;29(8):1–7.
[35] Gu Grace X, Libonati Flavia, Wettermark Susan D, Buehler Markus J. Printing nature: unraveling the role of nacre's mineral bridges. J Mech Behav Biomed Mater 2017;76(May):135–44.
[36] Askarinejad S, Rahbar N. Toughening mechanisms in bioinspired multilayered materials. J R Soc Interface 2014;12(102). 20140855–20140855.
[37] Cundall PA, Strack ODL. A discrete numerical model for granular assemblies. Geotechnique 1979;29(1):47–65.
[38] Dubois Frédéric, Radjai Farhang. Discrete-element modeling of granular materials. ISTE Ltd; 2011.
[39] Bruno Chareyre. The discrete element method for granular solids. first ed. edition. ISTE Press - Elsevier; 2019.

[40] Leclerc W. Discrete Element Method to simulate the elastic behavior of 3D heterogeneous continuous media W. Int J Solids Struct 2017.
[41] André Damien, Iordanoff Ivan, Charles Jean-luc, Néauport Jérôme. Discrete element method to simulate continuous material by using the cohesive beam model. Comput Methods Appl Mech Eng 2012. 213-216:113–125.
[42] André Damien, Mohamed Jebahi, Iordanoff Ivan, Charles Jean-luc, Néauport Jérôme. Using the discrete element method to simulate brittle fracture in the indentation of a silica glass with a blunt indenter. Comput Methods Appl Mech Eng 2013;265:136–47.
[43] Kumar Rishi, Rommel Sarshad, Jauffrès David, Lhuissier Pierre, Martin Christophe L. Effect of packing characteristics on the discrete element simulation of elasticity and buckling. Int J Mech Sci 2016;110:14–21.
[44] Maheo L, Dau F, André D, Charles JL, Iordanoff I. Composites : Part B A promising way to model cracks in composite using Discrete Element Method. Composites Part B 2015;71:193–202.
[45] Jauffrès David, Christophe L, Martin CL, Bordia RK Rajendra K. Design of strain tolerant porous microstructures – a case for controlled imperfection. Acta Mater apr 2018;148:193–201.
[46] Roussel Denis, Lichtner Aaron, Jauffrès David, Villanova Julie, Bordia Rajendra K, Martin Christophe L. Strength of hierarchically porous ceramics: discrete simulations on X-ray nanotomography images. Scr Mater 2016;113:250–3.
[47] Radi Kaoutar, Jauffrès David, Deville Sylvain, Martin Christophe L. Elasticity and fracture of brick and mortar materials with discrete elements simulations. J Mech Phys Solids 2019;126:101–16.
[48] Martin CLL, Bouvard D, Shima S. Study of particle rearrangement during powder compaction by the Discrete Element Method. J Mech Phys Solids 2003;51:667–93.
[49] Feilden Ezra, Giovannini Tommaso, Ni Na, Ferraro Claudio, Saiz Eduardo, Vandeperre Luc, Finn Giuliani. Micromechanical strength of individual Al2O3 platelets. Scr Mater 2017;(131):55–8.
[50] Anderson TedL. Fracture mechanics TextBook. third ed. edition 2005.
[51] Tada Hiroshi, Paris Paul C, George Irwin R. The stress analysis of cracks handbook. 1985.
[52] Davidson Paul, Anthony Waas M. Non-smooth mode I fracture of fibre-reinforced composites: an experimental, numerical and analytical study. 2011. p. 1942–65.
[53] Heid-Jorgensen Simon, Budzik Michal K. J Mech Phys Solids 2018;117(1–21).
[54] Hossain MZ, Hsueh C, Bourdin B, Bhattacharya K. Effective toughness of heterogeneous media. J Mech Phys Solids 2014;71:15–32.
[55] Yue Shao, Zhao Hong Ping, Feng Xi Qiao. Optimal characteristic nanosizes of mineral bridges in mollusk nacre. RSC Adv 2014;4(61):32451–6.
[56] Barthelat François, Li Chun Ming, Comi Claudia, Horacio D. Espinosa. Mechanical properties of nacre constituents and their impact on mechanical performance. J Mater Res 2006;21(8):1977–86.
[57] Song F, Soh AK, Bai YL. Structural and mechanical properties of the organic matrix layers of nacre 2003;24:3623–31.
[58] Martin CL. Elasticity, fracture and yielding of cold compacted metal powders. J Mech Phys Solids 2004;52:1691–717.